Available online at www.sciencedirect.com
ScienceDirect
Journal of Solid State Chemistry 181 (2008) 45–50
JOURNAL OF SOLID STATE CHEMISTRY
www.elsevier.com/locate/jssc

Long- and short-range order in stuffed titanate pyrochlores

G.C. Lau[a,*], T.M. McQueen[a], Q. Huang[b], H.W. Zandbergen[c], R.J. Cava[a]

[a]*Department of Chemistry, Princeton University, Princeton, NJ 08544, USA*
[b]*NIST Center for Neutron Research, NIST, Gaithersburg, MD 20899, USA*
[c]*Department of Materials Science, Delft University of Technology, Rotterdamseweg 137, 2682 AL Delft, The Netherlands*

Received 24 July 2007; received in revised form 17 October 2007; accepted 19 October 2007
Available online 11 December 2007

Abstract

We report a structural study of the stuffed pyrochlore series $Ln_2(Ti_{2-x}Ln_x)O_{7-x/2}$ (Ln = Ho, Yb; $0 \leqslant x \leqslant 0.67$). Electron microscopy and Rietveld refinements of neutron powder diffraction data for the $x = 0.67$ end members, Ho_2TiO_5 and Yb_2TiO_5, reveal that small domains (~50 Å or less) exist where the Ln and Ti/Ln sublattices are pyrochlore like, while the average structure is fluorite like. Both the Ho and Yb stuffed pyrochlore series for $0.1 \leqslant x \leqslant 0.5$ are shown to be a composite of long- and short-range-ordered pyrochlore phases. The relative fraction of long-range vs. short-range pyrochlore order decreases with increasing Ln doping. An additional complex structural modulation of the pyrochlore structure is observed in electron diffraction and high-resolution electron microscopy images.

Keywords: Pyrochlore; Stuffed pyrochlore; Stuffed spin ice; Geometrically frustrated magnet; Pyrochlore to fluorite solid solution; Rare-earth titanate

1. Introduction

Rare-earth titanate pyrochlores, with general formula $A_2B_2O_7$, have been studied extensively in the past decade as examples of geometrically frustrated magnets [1,2]. Lanthanide and titanium ions in these materials form two separate interpenetrating sublattices of corner sharing tetrahedra. This geometry of cations and the effective magnetic interactions in $Dy_2Ti_2O_7$ and $Ho_2Ti_2O_7$ give rise to unique magnetic properties that mimic the structural behavior of frozen water [3–7]. Frustration in these 'spin ice' pyrochlores suppresses long-range magnetic order down to the mK regime [5,7–9]. The disorder results in a non-zero entropy at 0 K [6,8,10] in accordance with predictions made by Pauling [11] for the same zero-point entropy observed in water ice [12,13].

Rare-earth titanate pyrochlores can be chemically altered by doping extra magnetic lanthanide atoms in place of non-magnetic Ti atoms to form the series $Ln_2(Ti_{2-x}Ln_x)O_{7-x/2}$ (Ln = Tb–Lu; $0 \leqslant x \leqslant 0.67$) [14]. The cubic pyrochlore structure is retained by rapidly quenching the materials from high temperature to avoid more thermodynamically stable phases at lower temperatures [14]. The 'stuffed' Ho titanates were shown to display the same residual entropy as regular spin ice despite the presence of additional Ho moments [15], and the average crystal structure was shown to undergo a pyrochlore to fluorite phase transition upon lanthanide stuffing [14,15]. Consequently, doping extra Ln ions appeared to disorder the normally separate Ln and Ti sublattices into one mixed cation lattice. In the disordered structure, the separate sublattices of corner sharing tetrahedra present in the pyrochlore supercell become equivalent, resulting in a lattice of edge sharing tetrahedra in the fluorite subcell. The retention of zero-point entropy was unexpected, as ice-like frustration is expected only for geometries of corner sharing tetrahedra of Ising spins with ferromagnetic interactions [16–18]. This warrants further study into the local cation ordering in these stuffed materials to better understand the observed properties.

Previous reports and phase diagrams show the average structure of the maximally stuffed titanate pyrochlores ($Ln_2(Ti_{1.33}Ln_{0.67})O_{6.67}$ or Ln_2TiO_5) to be fluorite [14,15,19,20]. However, recent evidence reveals short-range pyrochlore ordering in Ho_2TiO_5 [21]. The Ho and Ti atoms are not completely disordered as in a fluorite structure, but rather order locally: the original Ho lattice is unchanged,

*Corresponding author.
E-mail address: laugc@airproducts.com (G.C. Lau).

0022-4596/$ - see front matter © 2007 Elsevier Inc. All rights reserved.
doi:10.1016/j.jssc.2007.10.025

and all the extra doped Ho mixes only onto the Ti site. This maintains a separation between the pyrochlore A and B sites to preserve the superstructure in the short range.

Here, we report a detailed analysis of the crystal structures of the stuffed pyrochlore series $Ln_2(Ti_{2-x}Ln_x)O_{7-x/2}$ for Ln = Ho and Yb and $x = 0$–0.67. Rietveld refinements of powder neutron diffraction (ND) data for Ho_2TiO_5 and Yb_2TiO_5 quantitatively show that the rare-earth cations are ordered in a pyrochlore fashion in the short-range. The small pyrochlore-like domains are also seen in high-resolution electron microscopy (HREM) studies. For doping levels of x ranging from 0.1 to 0.5, long- and short-range pyrochlore ordering exists simultaneously. The relative phase fraction of short-range order increases with Ln stuffing until only short-range pyrochlore ordering exists for $x = 0.67$. Electron diffraction (ED) and HREM images are also shown for Ho_2TiO_5. Details in these images support the existence of locally ordered pyrochlore domains.

2. Experimental

$Ln_2(Ti_{2-x}Ln_x)O_{7-x/2}$ (Ln = Ho, Yb; $0 \leqslant x \leqslant 0.67$) materials were prepared by first thoroughly mixing stoichiometric amounts of Ho_2O_3 (Alfa Aesar, 99.9%) or Yb_2O_3 (Aldrich, 99.9%) with TiO_2 (Aldrich, 99.9%) in an agate mortar and pestle. The powders were pressed into a pellet, wrapped in molybdenum foil, heated at 1700 °C in a static argon atmosphere for 12 h, and quenched to room temperature in approximately 30 min. The argon atmosphere was achieved in a vacuum furnace first evacuated to about 10^{-6} Torr and then back-filled with argon (Airgas, 99.9%) to room pressure.

Samples were analyzed for phase purity by powder X-ray diffraction (XRD) using Cu$K\alpha$ radiation and a diffracted beam graphite monochromator. Heating representative samples in oxygen in a thermogravimetric analyzer indicated oxygen stoichiometries consistent with the presence of Ti^{4+} and Ln^{3+}. ND data were collected at the NIST Center for Neutron Research on the BT-1 powder neutron diffractometer with neutrons of wavelength 1.5403 Å produced by a Cu (311) monochromator. Collimators with horizontal divergences of 15′ and 20′ of arc were used before and after the monochromator, and a collimator with a horizontal divergence of 7′ was used after the sample. Data were collected in the 2θ range of 3–168° with a step size of 0.05°. Rietveld refinements of the structures were performed with FullProf 2000 and WinPlotR [22]. The neutron scattering amplitudes used in the refinements were 0.801, 1.2430, −0.344, and 0.580 ($\times 10^{-12}$ cm) for Ho, Yb, Ti, and O, respectively.

Electron microscopy analysis was performed with a Philips CM200 electron microscope having a field emission gun operated at 200 kV. Electron-transparent areas of specimens were obtained by crushing them slightly under ethanol to form a suspension and then by dripping a droplet of this suspension onto a carbon-coated holey film on a Cu or Au grid.

3. Results and discussion

Rietveld refinement fits to the ND data for Ho_2TiO_5 and Yb_2TiO_5 are shown in Fig. 1. In both cases, both sharp and broad peaks are present. These are representative of the fluorite subcell and the short-range-ordered pyrochlore supercell, respectively. The fluorite structure consists of cations randomly distributed in a face centered cubic array. The pyrochlore structure, in contrast, has an ordered $2 \times 2 \times 2$ supercell of the fluorite structure due to the distinction between the A and B cation sites. Thus, the peaks in the diffraction patterns are a combination of fluorite substructure peaks and additional pyrochlore superstructure peaks that appear with increasing intensity as the pyrochlore-type ordering becomes more developed.

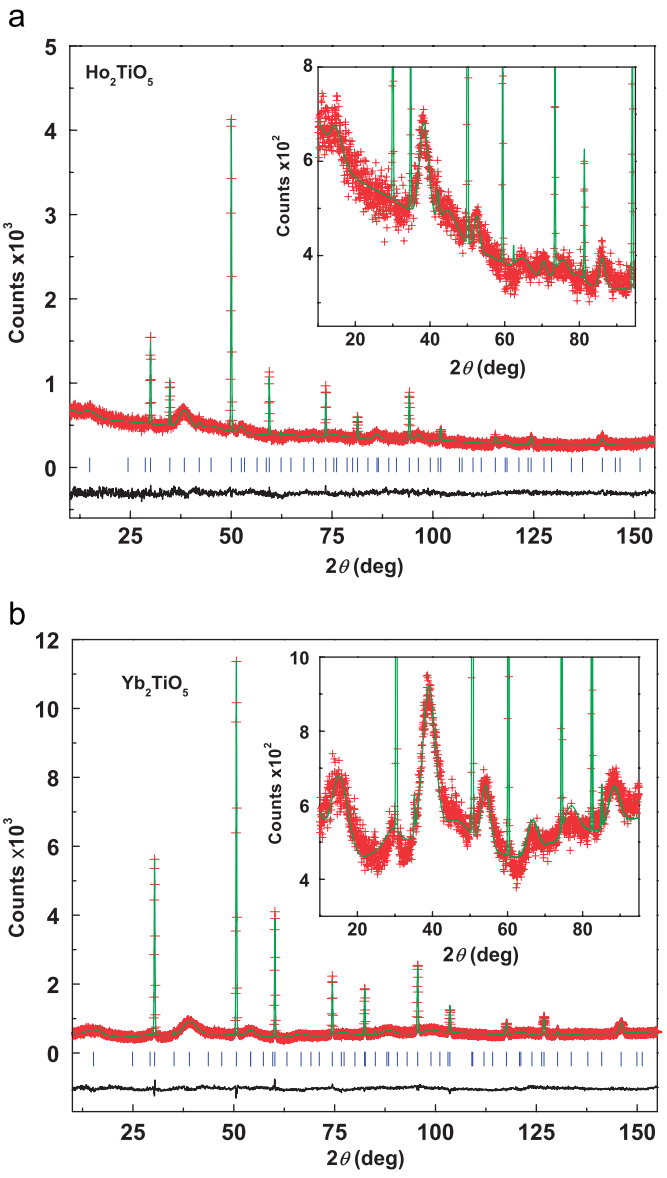

Fig. 1. Neutron powder diffraction data (crosses), Rietveld refinement fits (green), and difference curves (black) are shown in the main panels for Ho_2TiO_5 (a) and Yb_2TiO_5 (b). The insets enlarge a region to reveal the fits to the broadened pyrochlore peaks.

Table 1
Crystallographic data for Ho_2TiO_5 and Yb_2TiO_5 in the space group $Fd\bar{3}m$ (no. 227)

	(B_{iso} = isotropic displacement parameter; Occ = occupancy)						
	Atom	Wyckoff position	x	y	z	B_{iso} (Å^2)	Occ
Ho_2TiO_5	Ho(1)	16*d*	0.5	0.5	0.5	2.57(7)	1.0
	Ti(1)	16*d*	0.5	0.5	0.5	2.57(7)	0
	Ti(2)	16*c*	0	0	0	2.57(7)	0.70(2)
	Ho(2)	16*c*	0	0	0	2.57(7)	0.30(2)
	O(1)	8*b*	0.375	0.375	0.375	3.2(5)	0.94(9)
	O(2)	8*a*	0.125	0.125	0.125	3.2(5)	0.02(5)
	O(3)	48*f*	0.3424(8)	0.125	0.125	4.2(2)	0.95(1)
a (Å) = 10.3027(2) $\chi^2 = 1.11$; $R_{wp} = 5.32\%$; $R_p = 4.16\%$							
Yb_2TiO_5	Yb(1)	16*d*	0.5	0.5	0.5	2.57(3)	1.0
	Ti(1)	16*d*	0.5	0.5	0.5	2.57(3)	0
	Ti(2)	16*c*	0	0	0	2.57(3)	0.721(5)
	Yb(2)	16*c*	0	0	0	2.57(3)	0.279(1)
	O(1)	8*b*	0.375	0.375	0.375	1.9(2)	1
	O(2)	8*a*	0.125	0.125	0.125	1.9(2)	0
	O(3)	48*f*	0.3416(8)	0.125	0.125	4.6(1)	0.945
a (Å) = 10.1857(1) $\chi^2 = 2.03$; $R_{wp} = 5.64\%$; $R_p = 4.64\%$							

In previous reports employing only XRD [14,15], the broadened pyrochlore peaks were not observed, indicating that on average the Ln_2TiO_5 materials exhibit a fluorite structure. The presence of the broadened pyrochlore peaks in the ND data suggests that the oxygen atoms may play a significant role in the local ordering of the cations.

Fitting both sharp and broad peaks simultaneously in a Rietveld refinement can be problematic. Reports and methods exist in the literature where fits accommodate hkl -dependent (anisotropic) peak broadening due to microstrain [23–28]. However, to our knowledge, few examples are known for Rietveld fits to peak width differences of the magnitudes seen in the stuffed pyrochlores ($FWHM_{sharp}$~0.2°; $FWHM_{broad}$~2–4°). FullProf was used for the refinements due to the ability of the program to refine individual peak widths [26]; this is required due to the anisotropic peak broadening present (see ED pattern Fig. 4a). An 8-term polynomial was used to fit the background together with a Thompson Cox Hastings pseudo-Voigt function to describe the peak shape for all reflections. Site occupancies and isotropic atomic displacement parameters were fixed to reasonable values in the initial refinement cycles. Peak widths and shifts for individual broadened pyrochlore peaks were refined. When the broadened peaks and background were fit adequately by inspection (see insets, Figs. 1a and b), then all peak widths and shifts were fixed before refining site occupancies and atomic displacement parameters in the final refinement cycles. Cation occupancies were constrained to sum to the nominal stoichiometric ratios, and oxygen occupancies were constrained to maintain charge neutrality. Figs. 1a and b show the quality of the fits to be excellent.

Results from the refinements are given in Table 1. When freely refined, the A-site occupancies for both Ho_2TiO_5 and Yb_2TiO_5 showed that the A site of the pyrochlore structure was fully occupied by rare-earth atoms for both cases (i.e. the freely refined Ti occupancy on the A site was found to be −0.03(2) and 0.05(1), respectively; the occupancy was therefore set to 0 in the final refinement). The extra stuffed lanthanide ions mix exclusively with Ti on the B site. This distinction between A and B sites quantitatively shows that both Ho_2TiO_5 and Yb_2TiO_5 have the pyrochlore structure in the short-range. In the fluorite crystal structure, oxygen atoms randomly occupy the 8*b*, 8*a*, and 48*f* sites, designated as O(1), O(2), and O(3) sites in Table 1. The refinements of the occupancies of the oxygen sites for Ho_2TiO_5 and Yb_2TiO_5 reveal vacancies in the 48*f* positions for both cases, and in the Ho case, also for the 8*b* positions, consistent with the expected loss of oxygen due to charge neutrality considerations following the replacement of Ti^{4+} ions with Ln^{3+}. The O(2) 8*a* site is found in both cases to be vacant (freely refined to within one standard deviation of zero occupancy, 0.02(5), for the Ho case, and −0.01(5) in the Yb case and therefore set to zero), as is the case for a normal undoped pyrochlore. In addition, for the Yb case, the freely refined occupancy of the O(1) 8*b* site was within one standard deviation of full occupancy, 1.1(1), and therefore set to 1 in the final refinements; leaving an oxygen occupancy of 0.945 for the O(3) 48*f* site, fully defining the oxygen distribution. Thus the oxygen sublattice for both Ho and Yb compounds remains fully pyrochlore-like on rare-earth stuffing. The peak widths determined from the refinements give approximate domain sizes of 30 Å for Ho_2TiO_5 and 20 Å for Yb_2TiO_5. The largest intensity

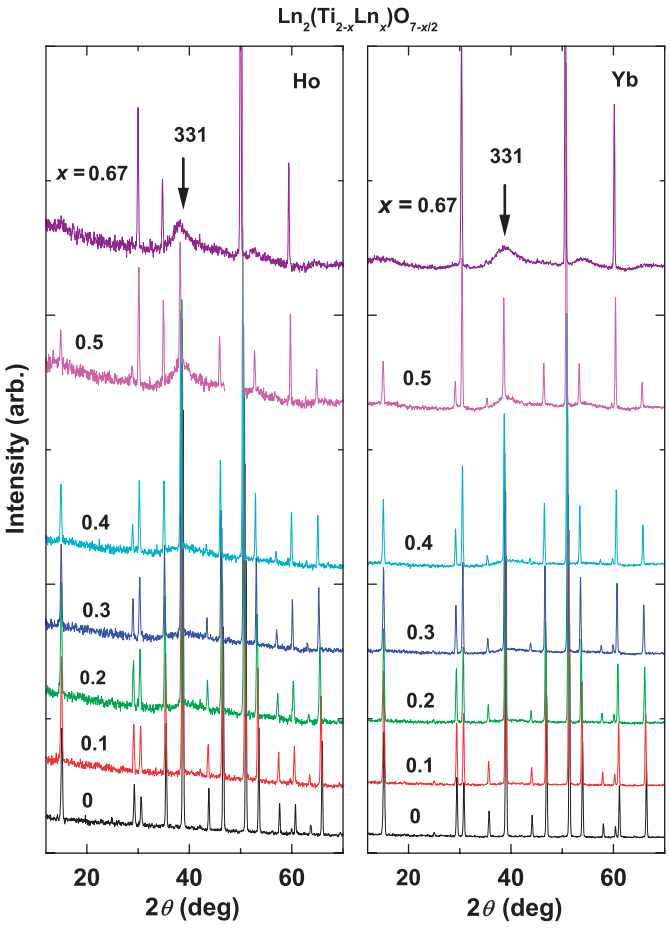

Fig. 2. Neutron powder diffraction data is displayed for the series $Ln_2(Ti_{2-x}Ln_x)O_{7-x/2}$, where Ln = Ho, Yb and x ranges from 0 to 0.67. The region around the (331) peak is emphasized to show the coexistence of sharp and broad diffraction for the (331) reflection. This indicates the simultaneous occurrence of long and short-ranged pyrochlore ordering as extra Ln atoms are doped in place of Ti. This is most apparent for the $x = 0.5$ doping level. At $x = 0.67$, pyrochlore ordering occurs only in the short range.

broadened pyrochlore reflections of both Ho_2TiO_5 and Yb_2TiO_5 were shifted from their ideal positions by 0.5° or less, significantly smaller than the FWHM values (2–4°). Fits performed without peak shifts did not result in significantly worse residuals, but gave unreasonable oxygen site occupancies. The peak shifts suggest that the broadened super-reflections are slightly incommensurate with the ideal pyrochlore supercell peak positions. Thermal displacement parameters for all elements refined to relatively large values. We attribute this to the correlation of the temperature factors with the positional disorder present on the cation B site and oxygen lattices as well as the broadening of all the pyrochlore peaks.

ND patterns are displayed in Fig. 2 for the rest of the $Ln_2(Ti_{2-x}Ln_x)O_{7-x/2}$ phases for both the Ho and Yb series. The 2θ range is focused around the (331) peak, the largest intensity pyrochlore reflection in the ND data. For $x = 0.1$–0.5, the (331) reflection is a combination of a sharp and broad peak. This indicates the coexistence of both long- and short-range pyrochlore ordering at those

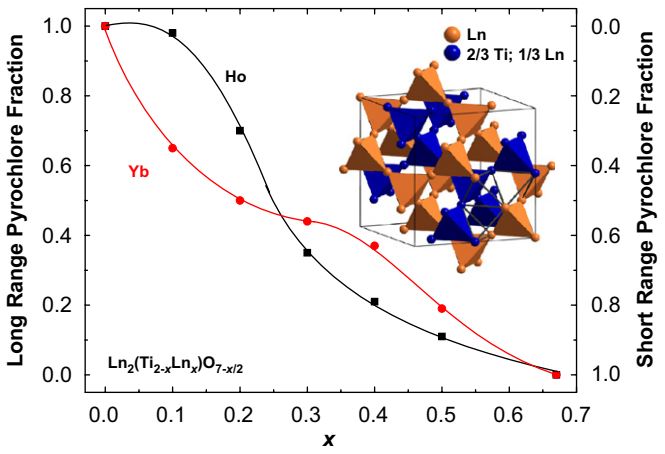

Fig. 3. Relative fractions of long-range versus short-range pyrochlore ordering in $Ln_2(Ti_{2-x}Ln_x)O_{7-x/2}$ are shown for the varying Ho or Yb doping levels. The approximate fractions are determined from the ratio of sharp to broad (331) peak areas. Lines are drawn as guides to the eye. Inset: the local ordering of the cation lattice is shown for Ln_2TiO_5 (Ln = Ho, Yb). Approximate site occupancies are given. Thicker bonds outline the coordination of edge sharing tetrahedra in the fluorite subcell.

compositions. We considered the possibility that the coexistence of sharp and broad peaks could be due to small pyrochlore crystallites precipitating out during rapid cooling within a larger particle having the Ln_2TiO_5 fluorite structure. This scenario would require the powder diffraction patterns for each doping level to show a set of sharp diffraction peaks fixed at 2θ values corresponding to the d-spacings of Ln_2TiO_5. However, the ND patterns for the doping series show that both sharp and broad peaks shift systematically to lower 2θ values with increasing doping. This indicates a solid solution of pyrochlore structure rather than a two-phase mixture of Ln_2TiO_5 and pyrochlore. Further, the electron miscoscope study indicated that the samples show only the presence of a uniform distribution of nanometer-size pyrochlore-like domains (see Fig. 4b), with no evidence for the presence of very small precipitates within a matrix of larger crystallites.

To approximate the phase fractions of long and short-range order, the (331) peak was fit with a pseudo-Voigt function as a combination of two peaks, one sharp and one broad. The ratio between the areas of the two individual peaks gives the approximate phase fractions. The fraction of long-range order as a function of stuffing level, x, is plotted in Fig. 3. A roughly linear decrease of long-range pyrochlore ordering (concurrent with the increase of short-range pyrochlore ordering) with respect to increasing stuffing is observed for both Ho and Yb materials, though there are subtle differences between the two cases. The Ho stuffed pyrochlore, for example, exhibits a larger proportion of long-range order at lower stuffing levels. This makes sense because the large size disparity between Ho and Ti should result in the tendency to maintain long-range ordering to a higher stuffing level. The inset of Fig. 3 depicts the local cation lattice of the stuffed materials. Although long-range pyrochlore ordering is lost upon Ln stuffing, the arrangement of

pure Ln on the A site and a mixture of Ln and Ti on the B site is maintained in the short range.

The ED pattern for Ho_2TiO_5 (Fig. 4a) shows the projection along the ⟨110⟩ zone axis. Three main features are noted: (1) the strongest spots represent reflections from the fluorite subcell, (2) the streaked reflections halfway in between fluorite spots in the (111) direction confirm the presence of short-range pyrochlore ordering, and (3) a minor structural modulation of the cubic pyrochlore structure is present, described by a seven-fold increase of the unit cell in the (662) direction. The first two features support the results of the Rietveld fits, where the materials order locally in the pyrochlore structure. The 7× supercell and HREM image (Fig. 4b) however, indicate that the details of the local ordering in Ho_2TiO_5 are actually more complicated. Domains of the pyrochlore ordering can be seen in the HREM image as fringes in the (111) direction. However, the fringes do not occur in the $(11\bar{1})$ direction inside this same domain, suggesting that due to the minor structural distortion the local symmetry within these small regions is no longer cubic. The same situation is observed for a region of the 7× superstructure where fringes are seen in the (662) direction but not the $(66\bar{2})$. With a 5 nm spot size, the ED picture is a composite of these domains, resulting in an average picture that fits a cubic pyrochlore structure. This lower symmetry in the local structure is consistent with the slightly shifted broadened peaks in the powder diffraction data discussed earlier. The ED patterns and structural images seen in these stuffed titanate systems, typified by Fig. 4, are remarkably similar to those seen in the $(1-x)ZrO_2{:}xLnO_{1.5}$ cubic zirconia systems near $x = 0.5$ [29], including the fact that the short range pyrochlore ordering that gives rise to the diffuse peaks in (111) directions appears to have one-dimensional character when looked at within a single nanometer-size domain. These domain sizes, ~50 Å or less, seen in the HREM are consistent with those determined from peak widths in the ND data; the domain images (Fig. 4b) show that the ordering within the domains is excellent and the domain boundaries are sharp. Peaks for the 7× supercell are not easily seen in the ND patterns, making the exact nature of this additional complex supercell unknown at this time. Further study would be of interest to clarify the complexity of this structural modulation, the apparent non-cubic symmetry of the small pyrochlore domains seen in the HREM, which suggests that the local structures could be related to $CaUO_4$ [30], and the similarities between the stuffed titanate pyrochlores and the lanthanide-stabilized cubic zirconias.

We argue that the formation of anti-phase domains is responsible for the structural observations described above. At high temperatures, doping extra Ln in $Ln_2Ti_2O_7$ causes disorder between cations across both A and B sites of the pyrochlore structure. As the material is quenched, Ln and Ti will tend to separate onto different sites due to the large size difference between atoms. The consequence is the formation of a pure Ln site that nucleates out of one of the two lattices of interpenetrating corner sharing tetrahedra in the high-temperature disordered fluorite. This pure Ln site locally becomes the A site of the pyrochlore structure, while the Ti and remaining Ln ions are forced to mix together onto the B site. Small antiphase domains result from the pure Ln site locally picking either one or the other of the interpenetrating lattices of tetrahedra, frozen in by the rapid quench before the ordered regions grow beyond

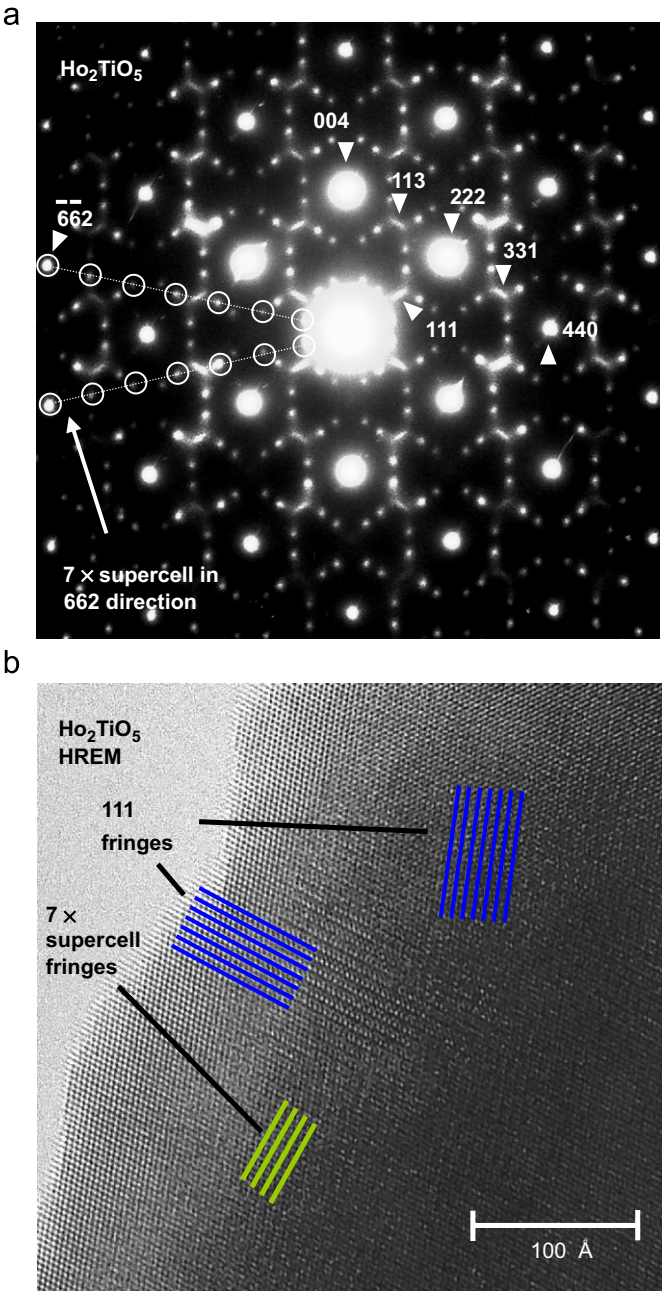

Fig. 4. (a) The ⟨110⟩ zone axis electron diffraction pattern is shown for Ho_2TiO_5. The reflections are indexed with respect to a cubic pyrochlore structure. Pyrochlore reflections are streaked in the ⟨111⟩ directions, consistent with short-range ordering. An additional complex modulation of the pyrochlore structure consisting of a seven-fold enlargement of the unit cell in the (662) direction is observed. (b) A HREM image of Ho_2TiO_5 reveals the ⟨111⟩ fringes of short-range ordered pyrochlore domains. Fringes for a domain of the 7× supercell are shown also. The pyrochlore regions order over a distance of about 50 Å or less.

~50 Å in scale. A powder average of many antiphase domains results in the apparent disorder of A and B sites, giving the fluorite subcell in the long range. These small domains are clearly seen in electron microscope images, and are shown in Fig. 4b). It was shown previously that slower cooling of these materials allows the local ordering to anneal into larger domains, resulting in the observation of long-range pyrochlore ordering even for the $x = 0.67$ (Ho_2TiO_5) sample [21]. The existence of pyrochlore ordering is not entirely unexpected. Cation disorder to form fluorite-type structures occurs, for example, in zirconate pyrochlores where the A and B cations are closer in size [29–34]. The large size difference between Ln ions and Ti predispose them to naturally occupy different sites, resulting in the local pyrochlore domains.

The relative proportion of these short-range-ordered antiphase domains versus long-range ordering is composition dependent. We surmise that for the undoped pyrochlore, there is no disorder between cations at high temperature. Thus, upon quenching, only long-range pyrochlore ordering exists. As more Ln is stuffed into the structure, the degree of cation mixing increases proportionally at high temperatures. This results in the increasing phase fraction of short-range pyrochlore ordering through the formation of antiphase domains, as described. Ho, which has a greater size disparity with Ti than does Yb, would not mix as easily with Ti. The Ho compounds therefore exhibit less disorder even at high temperature. This is consistent with the trend seen in Fig. 3 where long-range order degrades more rapidly with stuffing for the Yb version.

4. Conclusions

ND data for the stuffed pyrochlores, $Ln_2(Ti_{2-x}Ln_x)O_{7-x/2}$ (Ln = Ho, Yb; $0 \leqslant x \leqslant 0.67$), are presented. Rietveld refinement on the ND patterns of the $x = 0.67$ end members, Ho_2TiO_5 and Yb_2TiO_5, reveal that pyrochlore ordering occurs in the short range for these families of stuffed rare-earth titanates. Although only Ho and Yb stuffed phases were analyzed due to their low neutron absorption cross-sections, we surmise that all the small rare-earth (Ho–Lu) stuffed pyrochlores have similar structures. Antiphase domains (~50 Å in size) exist where the pyrochlore A site is comprised of pure Ln atoms, and the B site is a mixture of Ti and the remaining stuffed Ln. The main features in the high-resolution image of Ho_2TiO_5 confirm the existence of short-range-ordered pyrochlore domains. A complex minor structural modulation of the cubic pyrochlore structure is also present. This modulation, coupled with observations in the HREM image of Ho_2TiO_5, suggest a subtle breaking of the cubic symmetry within the small antiphase domains.

Acknowledgments

This work was supported by the National Science Foundation Division of Materials Research (DMR-0353610). T.M. McQueen gratefully acknowledges support by the National Science Foundation Graduate Research Fellowship program. Certain commercial chemicals and equipment are identified in this report to describe the subject adequately. Such identification does not imply recommendation or endorsement by the NIST, nor does it imply that the equipment identified is necessarily the best available for the purpose.

References

[1] H.T. Diep, Frustrated Spin Systems, World Scientific, Singapore, 2004.
[2] J.E. Greedan, J. Alloys Compds. 408 (2006) 444–455.
[3] S.T. Bramwell, M.J.P. Gingras, Science 294 (2001) 1495–1501.
[4] M.J. Harris, S.T. Bramwell, D.F. McMorrow, T. Zeiske, K.W. Godfrey, Phys. Rev. Lett. 79 (1997) 2554–2557.
[5] K. Matsuhira, Y. Hinatsu, K. Tenya, T. Sakakibara, J. Phys. Condens. Matter 12 (2000) L649–L656.
[6] A.P. Ramirez, A. Hayashi, R.J. Cava, R. Siddharthan, B.S. Shastry, Nature 399 (1999) 333–335.
[7] J. Snyder, B.G. Ueland, J.S. Slusky, H. Karunadasa, R.J. Cava, P. Schiffer, Phys. Rev. B 69 (2004) 064414.
[8] S.T. Bramwell, M.J. Harris, B.C. den Hertog, M.J.P. Gingras, J.S. Gardner, D.F. McMorrow, A.R. Wildes, A.L. Cornelius, J.D.M. Champion, R.G. Melko, T. Fennell, Phys. Rev. Lett. 87 (2001) 047205.
[9] R. Higashinaka, H. Fukazawa, Y. Maeno, Phys. Rev. B 68 (2003) 014415.
[10] A.L. Cornelius, J.S. Gardner, Phys. Rev. B 6406 (2001) 060406.
[11] L. Pauling, J. Am. Chem. Soc. 57 (1935) 2680–2684.
[12] W.F. Giauque, M.F. Ashley, Phys. Rev. 43 (1933) 81–82.
[13] W.F. Giauque, J.W. Stout, J. Am. Chem. Soc. 58 (1936) 1144–1150.
[14] G.C. Lau, B.D. Muegge, T.M. McQueen, E.L. Duncan, R.J. Cava, J. Solid State Chem. 179 (2006) 3126–3135.
[15] G.C. Lau, R.S. Freitas, B.G. Ueland, B.D. Muegge, E.L. Duncan, P. Schiffer, R.J. Cava, Nat. Phys. 2 (2006) 249–253.
[16] S.V. Isakov, R. Moessner, S.L. Sondhi, Phys. Rev. Lett. 95 (2005) 217201.
[17] B.S. Shastry, Phys. B Condens. Matter 329 (2003) 1024–1027.
[18] R. Siddharthan, B.S. Shastry, A.P. Ramirez, A. Hayashi, R.J. Cava, S. Rosenkranz, Phys. Rev. Lett. 83 (1999) 1854–1857.
[19] G.V. Shamrai, R.L. Magunov, L.V. Sadkovskaya, I.V. Stasenko, I.P. Kovalevskaya, Inorg. Mater. 27 (1991) 140–141.
[20] G.V. Shamrai, A.V. Zagorodnyuk, R.L. Magunov, A.P. Zhirnova, Inorg. Mater. 28 (1992) 1633–1635.
[21] G.C. Lau, B.G. Ueland, M.L. Dahlberg, R.S. Freitas, Q. Huang, H.W. Zandbergen, P. Schiffer, R.J. Cava, Phys. Rev. B 76 (2007) 054430.
[22] J. Rodriguez-Carvajal, Abstracts of the Satellite Meeting on Powder Diffraction of the XV Congress of the IUCr, 1990, p. 127.
[23] P. Onnerud, Y. Andersson, R. Tellgren, P. Nordblad, F. Bouree, G. Andre, Solid State Commun. 101 (1997) 433–437.
[24] P. Sahu, J. Appl. Crystallogr. 38 (2005) 112–120.
[25] J. Rodriguezcarvajal, M.T. Fernandezdiaz, J.L. Martinez, J. Phys. Condens. Matter 3 (1991) 3215–3234.
[26] J. Rodriguez-Carvajal, T. Roisnel, European Powder Diffraction Epdic 8, vol. 443–444, 2004, pp. 123–126.
[27] N.C. Popa, J. Appl. Crystallogr. 31 (1998) 176–180.
[28] A. Leineweber, J. Appl. Crystallogr. 39 (2006) 509–518.
[29] Y. Tabira, R.L. Withers, J.C. Barry, L. Elcoro, J. Solid State Chem. 159 (2001) 121–129.
[30] R.L. Withers, J.G. Thompson, P.J. Barlow, J.C. Barry, Austr. J. Chem. 45 (1992) 1375–1395.
[31] S. Garcia-Martin, M.A. Alario-Franco, D.P. Fagg, A.J. Feighery, J.T.S. Irvine, Chem. Mater. 12 (2000) 1729–1737.
[32] S. Garcia-Martin, M.A. Alario-Franco, D.P. Fagg, J.T.S. Irvine, J. Mater. Chem. 15 (2005) 1903–1907.
[33] Y. Liu, R.L. Withers, L. Noren, J. Solid State Chem. 177 (2004) 4404–4412.
[34] R.L. Withers, J.G. Thompson, P.J. Barlow, J. Solid State Chem. 94 (1991) 89–105.